IVYSPRING INTERNATIONAL PUBLISHER

Theranostics

2018; 8(15): 4072-4085. doi: 10.7150/thno.25357

Research Paper

Bioluminescence imaging and two-photon microscopy guided laser ablation of GBM decreases tumor burden

Yingwei Fan[1*], Yu Sun[2*], Wei Chang[1], Xinran Zhang[1], Jie Tang[2], Liwei Zhang[2]✉, Hongen Liao[1]✉

1. Department of Biomedical Engineering, School of Medicine, Tsinghua University, Beijing 100084, China
2. Department of Neurosurgery, Beijing Tiantan Hospital, Capital Medical University, Beijing, 100050 China

* These authors contributed equally to this manuscript.

✉ Corresponding authors: Prof. Hongen Liao, Email: liao@tsinghua.edu.cn and Dr. Liwei Zhang, Email: zlwtt@aliyun.com

Received: 2018.02.04; Accepted: 2018.05.03; Published: 2018.07.16

Abstract

Brain tumor delineation and treatment are the main concerns of neurosurgeons in neurosurgical operations. Bridging the gap between imaging/diagnosis and treatment will provide great convenience for neurosurgeons. Here, we developed an optical theranostics platform that helps to delineate the boundary and quantitatively analyze glioblastoma multiforms (GBMs) with bioluminescence imaging (BLI) to guide laser ablation, and we imaged the GBM cells with two-photon microscopy (TPM) to visualize the laser ablation zone *in vivo*.

Methods: Laser ablation, using the method of coupled ablated path planning with the guidance of BLI, was implemented *in vivo* for mouse brain tumors. The mapping relationship between semi-quantitative BLI and the laser ablation path was built through the quantitative tumor burden. The mapping was reflected through coupled ablated path planning. The BLI quantitatively and qualitatively evaluated treatment using laser ablation with the appropriate laser parameters and laser-tissue parameters. These parameters were measured after treatment. Furthermore, histopathological analysis of the brain tissue was conducted to compare the TPM images before and after laser ablation and to evaluate the results of *in vivo* laser ablation. The local recurrences were measured with three separate cohorts. The weights of all of the mice were measured during the experiment.

Results: Our *in vivo* BLI data show that the tumor cell numbers were significantly attenuated after treatment with the optical theranostics platform, and the delineation of GBM margins had clear views to guide the laser resection; the fluorescence intensity *in vivo* of GBMs quantitatively analyzed the rapid progression of GBMs. The laser-tissue parameters under guidance of multimodality imaging ranged between 1.0 mm and 0.1 mm. The accuracy of the laser ablation reached a submillimeter level, and the resection ratio reached more than 99% under the guidance of BLI. The histopathological sections were compared to TPM images, and the results demonstrated that these images highly coincided. The weight index and local recurrence results demonstrated that the therapeutic effect of the optical theranostics platform was significant.

Conclusion: We propose an optical multimodality imaging-guided laser ablation theranostics platform for the treatment of GBMs in an intravital mouse model. The experimental results demonstrated that the integration of multimodality imaging can precisely guide laser ablation for the treatment of GBMs. This preclinical research provides a possibility for the precision treatment of GBMs. The study also provides some theoretical support for clinical research.

Key words: minimally invasive optical theranostics, laser ablation, bioluminescence imaging, two-photon microscopy, GBM resection, multimodality guided surgery

Introduction

Glioblastoma multiforms (GBMs) severely affect the health of human beings and threaten the lives of patients. Surgery is one of the current treatments for brain tumors, such as brain glioma resections [1]. A conventional surgeon's experience-based resection has limits regarding the identification of cancer and non-cancer so that precision surgery cannot be quantitatively implemented in neurosurgery. Image-guided surgical resection has been developed for neurosurgical resection [2]. A cellular imaging technique will more precisely guide the resection of GBMs [3]. Image-guided surgery and/or other treatments are emerging and being translated as the main treatment of orthotopic GBMs.

Laser ablation can be used in minimally invasive surgery for diseased tissue. Intraoperative laser ablation has been proposed for neurosurgical resection, and the results of laser ablation have been evaluated and compared to those of neurosurgical resection [4, 5]. As a new tool, laser ablation is used as an alternative surgery for brain tumors [6]. It uses heat effects from laser probes to destroy cancerous tissue. Stereotactic laser ablation has also been used in the focal treatment of high-grade glioma [7] and recurrent high-grade glioma [6, 8]. Advances in probe design, cooling mechanisms, and intraoperative imaging and real-time diagnosis have increased the utilization of lasers in neurosurgical treatment [5, 9]. *In vivo* laser ablation of mouse brain tumors has been implemented [10]. Laser resection for brain tumors can result in high accuracy and provide an alternative approach for the treatment of brain tumors. Current various biomedical technologies in neurosurgery have been used to detect brain gliomas or GBMs. These technologies include intraoperative magnetic resonance imaging (MRI) [11], intraoperative computer tomography (CT) [12], ultrasound imaging [13], Raman imaging [14-16], optical coherence tomography (OCT) [17], intraoperative spectroscopy [18], hyperspectral brain imaging [19], and intraoperative fluorescence imaging [20]. Furthermore, mass spectrometry [21] and 5-amino-levulinic acid (5-ALA) fluorescence measurement and the corresponding spectral analysis technique [22, 23] have been applied for the identification of tumorous tissues and for the guidance of brain tumor laser ablation.

Advances in intraoperative imaging and navigation have increased laser ablation applications into resections of GBMs, especially magnetic resonance-guided laser ablation [24] and OCT-guided laser ablation [25]. For residual cancer removal, a fluorescence-guided laser ablation system, which can resect residual cancer in a mouse model, has been proposed by Lazarides [26]. Furthermore, for imaging and guiding treatment of orthotopic glioma, bioluminescence imaging (BLI) has been widely used for the evaluation of treatment efficiency [27-29]. It has been combined with photoacoustic imaging (PAI) guided surgery using a multifunctional targeted nanoprobe [30]. To monitor the tumor development and progression, BLI is also used as a non-invasive technical tool for evaluating and optimizing therapeutic efficacy [31]. The tumor-activatable theranostic nanomedicine platform was developed for near-infrared fluorescence-guided surgery and combinatorial phototherapy [32]. In previous research, we developed the integration of OCT and a laser ablation system [25] for precise treatment of soft biological tissue. For microscopic imaging, two-photon microscopy (TPM) can image the subcellular biological tissue. Miniatured TPM has been proposed for monitoring brain function in the freely moving mouse [33]. The combination of TPM imaging and coherence anti-Stokes Raman scattering (CARS) microscopy is used for delineating the brain orthotopic tumor margin. To bridge the gap of fundamental research and clinical applications of laser ablation in the treatment of *in vivo* brain orthotopic tumor, TPM and confocal microscopy have been applied for evaluating the human sclera after femtosecond laser ablation [34]. In neurosurgical treatment, the identification of cancerous and normal tissue can precisely guide resection of the cancerous tissue and completely reserve non-cancerous tissues or structures. In multi-modality imaging-guided laser ablation, the combination of microscopic and macroscopic imaging will guide more precise laser ablation of brain tumors.

To address the issue, we used multimodality imaging, which included BLI and TPM, to image the suspected tumorous tissue and provide microscopic images. With multimodality imaging guidance, laser ablation was conducted and coupled with the planning of thermal effects to treat brain tumors in a mouse model. In this research, we created the mouse model by injecting human GBM cells into the mouse brain tissue. We developed a mathematical model of laser ablation with different incident angles and heights of a fiber probe. Then, guided by the quantitative delineation of the tumor boundary and tumor burden and using the appropriate laser parameters, we implemented laser ablation with coupled ablated path planning in a mouse model. The BLI results demonstrated that the laser ablation results had significant attenuation. The laser ablation results demonstrated that the ablation accuracy reached a submillimeter size, which provided a result of 0.1 mm resection accuracy. Multimodality

imaging-guided laser ablation can provide the potential translation of cross-scale imaging and laser ablation for treating the *in vivo* and *in situ* GBMs.

Methods

System configuration and flowchart

We acquired human GBM cells and label them with luciferase-GFP by transfection with lentivirus vector (**Figure 1**). These murine cells were cultured for approximately four weeks. The laser ablation of GBMs, which requires preoperative boundary delineation of the GBM, was integrated into a multimodality technique for detecting GBMs in a mouse model.

We used whole-body BLI and TPM imaging to image before and after laser ablation. We conducted laser ablation with the guidance of BLI, and the path planning of the laser was conducted by coupling the laser parameters and the tissue ablation parameters. Furthermore, the TPM images were acquired and compared to the histopathological sections for the evaluation of the laser ablation results.

Bioluminescence imaging, two-photon microscopy, and laser ablation modeling

Bioluminescence imaging module

D-luciferin was injected through bulbus oculi, and imaging was implemented before and after laser ablation. To solve the photobleaching issue, we tested the imaging with BLI and automatically computed the fluorescence intensity. The analytical results of the bioluminescence images, when compared with the intraoperative scenes, showed the fluorescence intensity excited by the visible light, which was located in GBM cells and delineated the margin with reliable accuracy.

Before the BLI, the mouse body weight was also measured. The changes in body weight of the treated mice demonstrated the brain orthotopic tumor progression. Furthermore, the preoperative BLI also delineated the orthotopic GBM and provided the fluorescence intensity of GBMs for resection with laser ablation.

Two-photon microscope (TPM) module

TPM has been widely used in biomedical imaging on a microscopic level, especially for neurological functions [35] and the progression of GBM cells. For the imaging of microscopic tumor cells, TPM has great application potential. The brain orthotopic glioma have been imaged in an *in vivo* mouse model [36, 37]. *In vivo* subcellular imaging has high resolution, which demonstrates the invasion and enrichment of tumor cells.

The TPM module can visualize tumor cells *in vivo* with GFP in the mouse brain. We used the TPM module to image GBM cells at the location of orthotopic brain tumors. Evaluation of the GBM invasion was also conducted by visualizing the glioma cells. We chose different views for imaging the tumor cells based on the delineation of the tumor

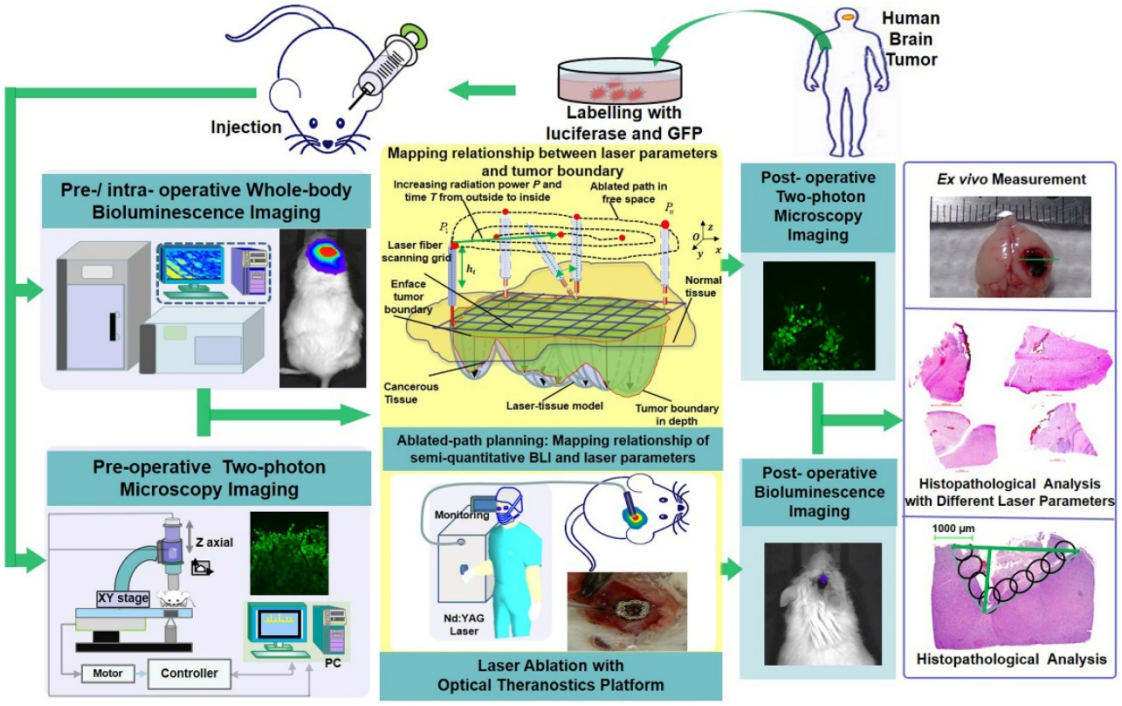

Figure 1. The configuration and flowchart of the optical theranostics platform for the laser ablation of GBMs *in vivo* with whole body bioluminescence imaging and a TPM imaging module. The histological section was evaluated and analyzed.

margin. The field of view is located within the location of the GBM margin.

Laser ablation module

The laser ablation module conducted the ablated light to the tissue surface through a multimode fiber. The mathematical modeling was simulated into the semi-ellipsoidal model [25]. In the laser ablation module, the fiber probe had two types of diameters: φ = 1.00 mm and φ = 0.75 mm.

The *in vivo* laser ablation of a tumor requires appropriate radiation power, *P*, and radiation duration, *T*, to perform a proper ablation. In our previous research [25], these parameters of laser radiation were evaluated in *ex vivo* soft biological tissue, and the laser-tissue parameters included the horizontal and longitudinal parameters: *a*, *b*, and *c*. In the semi-ellipsoidal modeling, we set the horizontal parameters as *a* = *b*. In this study, we simulated the mathematical modeling by adding two influencing factors: the height between the fiber probe and the tissue surface and the angle of the fiber probe. For directly quantitating laser parameters of this platform, the parameters were calculated with a reference value that is the output by the laser, such as the radiation power and radiation duration.

Brain orthotopic glioma and cell preparation in an *in vivo* mouse model

The human GBM cell line U87MG was obtained from the American Type Culture Collection. The cell line was maintained in McCoy's 5A medium supplemented with 10% fetal bovine serum and 1% penicillin at 37 °C with 5% CO_2. U87MG was transduced with lentiviral vectors containing luciferase and the GFP as previously described [38]. Flow cytometry was used to sort out the GFP positive U87MG cells. GFP and luciferase modified U87MG cells were prepared for the establishment of an orthotopic xenograft mouse model. The cells were harvested by trypsinization with 0.25% trypsin-EDTA (Gibco®). We washed the cells with phosphate-buffered saline (PBS) and centrifuged them at a speed of 300 ×g for 5 min.

This study was approved by the Institutional Animal Care and Use Committee (IACUC) of Tsinghua University, and all of the experimental procedures were performed in accordance with the guidelines of the IACUC. The animal experimental facility has been accredited by the Association for Assessment and Accreditation of Laboratory Animal Care International (AAALAC). A total of 8 NOD SCID-IL2R-γ chain–deficient (NSG) mice of 6-8 weeks of age were anesthetized with an intra-peritoneal injection of 2.5% avertin (Sigma) at a dose of 240 mg/kg. These mice were positioned on a stereotactic frame. An approximate 5 mm diameter craniotomy was performed on the right parietal bone. A total of 5×10^5 cells suspended in 10 μL of PBS were injected into the cortex of the parietal lobe at approximately 1 mm below the brain surface. The bone window was not closed in this research. We sutured the wound for the next therapy with the optical theranostics platform.

Coupled ablated path planning of *in vivo* orthotopic GBMs under the guidance of BLI

We used the whole-body BLI module (**Figure 2A**) to detect and delineate GBMs in the *in vivo* mouse model and then guided the laser ablation for the treatment of GBMs. The fluorescence intensity of the bioluminescence imaging results in a decision regarding laser parameters. The laser parameters included the radiation power, *P*, the radiation duration, *T*, the height between the laser-fiber tips and the tissue surface, *H* and incident angle, *θ* (**Figure 2B**). Furthermore, the tissue-ablation parameters included the horizontal parameters *a* and *b* and the longitudinal parameter *c*. For computational convenience, we hypothesized that the horizontal parameters *a* and *b* were equivalent, and thus, we measured the horizontal and longitudinal parameters *a* and *c*, respectively. These parameters reflected the invasion and thermal damage of laser ablation to the *in vivo* GBM. Multipoint laser ablation was coupled in an *in vivo* brain tumor as shown in **Figure 2C**.

For the purpose of choosing the appropriate laser parameters, we designed the experimental situation to implement the laser ablation of *in vivo* orthotopic glioma at different heights and angles and then measured the laser-tissue parameters, which included the horizontal parameters and the longitudinal parameters. For guiding the laser ablation with fluorescence intensity and tumor delineation, the delineation size of the tumor provided the path planning, and the fluorescence intensity decided the laser parameters (**Figure 2D**). We chose the appropriate state space of the laser-fiber probe motion based on tumor boundary with semi-quantitative BLI and set the ablated center P_1 by evaluating the tumor area. The laser probe followed the planning path and then reached the end-center P_n.

The laser parameters were increased from outside to inside by manipulating the control interface. This procedure will change with the tumor delineation and the laser parameters. Path planning based on the guidance of multimodality imaging could provide precision ablation of the orthotopic GBM. Ablated points are coupled together as a continuous track to excise large-scale orthotopic

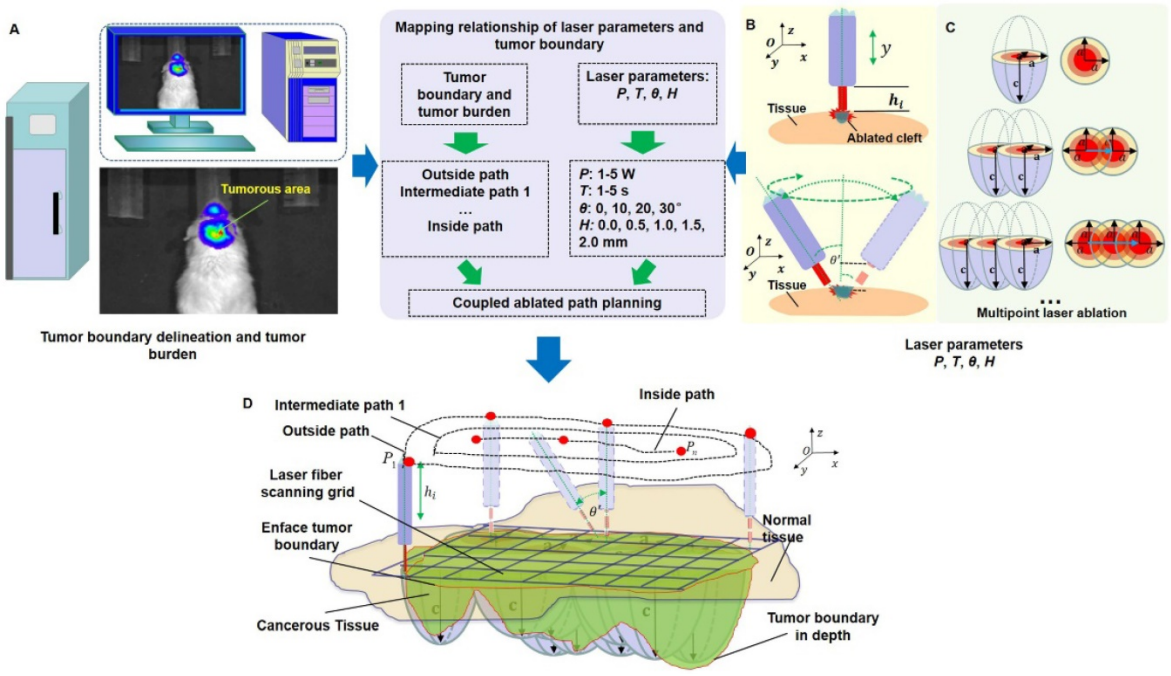

Figure 2. The path planning of the laser ablation *in vivo*. (A) The whole-body bioluminescence imaging *in vivo*. **(B)** The different heights between the fiber tip and tissue surface within the perpendicular incidence and the different incidence angles of the fiber probe. **(C)** The multipoint-coupled ablation model. **(D)** The mapping relationship between the laser parameters and the tumor boundary with semi-quantitative BLI.

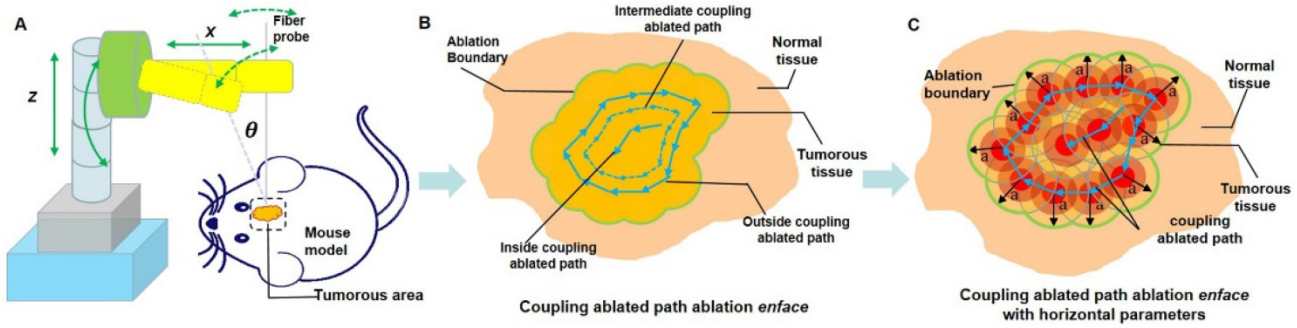

Figure 3. (A) The laser ablation of GBMs with the guidance of BLI. **(B)** The path planning of laser ablation. **(C)** The path planning of laser ablation with appropriate parameters. The green line stands for the automatic tumor margin, and the blue line stands for path planning.

gliomas. We call this laser ablation method coupled ablated path planning. The parameters of ablation modeling and the coupled ablated path are decided by the fluorescence intensity and the delineation of the GBMs. In this study, the appropriate laser parameters are chosen based on previous research as described in the experimental section. Coupled ablated-path planning was implemented with semi-quantitative BLI and tumor burden. This procedure of coupled ablated-path planning is shown in **Figure 3A-C** as follows:

First, the laser fiber probe follows the tumor boundary delineation from the semi-quantitative BLI, and the outside coupled ablation path is formed. A radiation power of 1 W and radiation duration of 1 s are initiated as the laser parameters.

Second, the theranostics platform provides increased radiation power by up to 5 W from the outside to the central point of the ablated path, which is when the laser fiber probe moves from outside the coupled ablated path to inside the coupled ablated path.

Third, the radiation duration changes with intraoperative ablation from the boundary area to the central-point location. The key point is that the tumor boundary ablation is usually performed at a lower power, shorter duration and higher fiber probe height.

Finally, laser resection is terminated when the tumorous tissue disappears in the central-point location.

Two-photon microscopy and histopathological section preparation

TPM imaging was conducted pre- and post-laser ablation. The matched location was as close to the location of the histopathological section through the flattened imaging plane of the *in vivo* mouse GBMs.

As the TPM only displayed tumor cells, normal cells cannot be shown in the TPM images. Furthermore, the TPM can show two-dimensional and three-dimensional images.

Preparation for histopathological analysis of the tissue included conventional hematoxylin and eosin (H&E) and histological processing: fixing, dehydrating, paraffin inclusion, *etc*. The pathological section was approximately located at the TPM imaging location. However, the pathological location did not completely match the imaging location, so we chose an approximate location for implementing the histological section. Although this issue still exists, we avoided additional location error as much as possible by labeling the feature points.

Local recurrence rates through the treatment of an optical theranostics platform

All of the mice were divided into three cohorts, which included healthy mice (tumor-/ablation-), neoplastic and nontreated mice (tumor+/ablation-), and neoplastic and treated mice (tumor+/ablation+) as shown in **Figure 9A**. The mice were placed into the optical theranostics platform under anesthesia, and a gross total tumor resection was performed with BLI-guided laser ablation. In the first cohort, healthy mice were normally raised, and the surgical wound was closed after craniotomy. In the second cohort, the mice were injected with tumor cells, and the surgical wound was closed. They were then raised in the experimental environment until all of the neoplastic mice were dead. In the third cohort, the mice were injected with tumor cells, and the surgical wound was closed. Laser ablation was performed, and these mice were raised until death. All of the mice were monitored for local recurrence over approximately 60 days. The weights of all of the mice were measured in the different groups. The Log-rank (Mantel-Cox) test was performed to compare the statistical significance of the survival curve of different cohorts.

Results

Laser ablation has been implemented with an optical theranostics system [25] in *ex vivo* diseased biological tissue as exploratory research. For the treatment of GBMs, the *in vivo* laser ablation-related parameters must be measured, and therefore, experiments with mice were performed in accordance with the Tsinghua University Experiment Animal Center-approved animal protocols (No. 17-LHE1).

System and experimental setup

In this study, we used a multimodal imaging module for the guidance and evaluation of laser ablation results of treatment of *in vivo* GBMs in a mouse model. Multimodality imaging included bioluminescence and TPM imaging. The laser ablation module was the main therapy method and the key to treatment of orthotopic GBMs (**Figure 4A-C**). The BLI module was used for *in vivo* detection and delineation of GBMs and guidance of the GBM resection in a mouse model. It was used as a noninvasive tool for monitoring the progression of GBMs (**Figure 4D**). The TPM was used for *in vivo* monitoring and evaluating

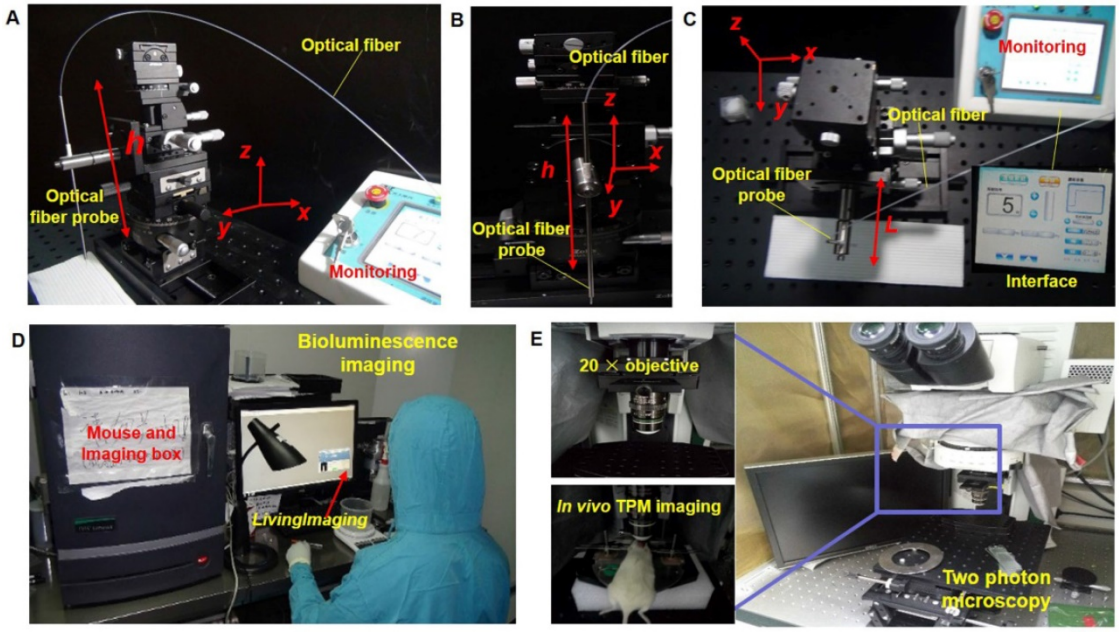

Figure 4. Module setup of the laser ablation with *in vivo* BLI and TPM imaging. (A-C) The laser ablation module in different observations, with the interface providing the output value of the radiation power and output mode. **(D)** The whole-body BLI module. **(E)** The TPM imaging module with a 20× objective and the *in vivo* TPM of mouse brain tumors.

the concentration of the GBM cells before and after laser ablation (**Figure 4E**). The output parameters of a Nd:YAG laser were decided by semi-quantitative BLI, which has a fluorescence intensity and tumor boundary.

Using the *in vivo* whole-body BLI module (Lumina II, PerkinElmer, US), we acquired the fluorescence intensity. The minimum image pixel resolution of the fluorescence image is approximately 50×50 μm^2 in the horizontal direction. All BLI results were processed with *LivingImaging* software. This processing included the delineation of GBM margins, and the computer automatically determined the fluorescence intensity. Laser resection included the two components. An optical fiber was used as the transference path for the Nd:YAG laser source with a wavelength of 1,064 nm (HGL-MY100C, Wuhan Huagong Laser Engineering, China) in the laser ablation module. The laser ablation module includes a near-infrared light source, which was a diode-pumped solid-state laser. The power was adjustable from 1 W to 75 W. To acquire the histopathological sections of GBMs and brain specimens, we used an automatic digital slide-scanning system (Axio Scan.Z1, Zeiss, Germany) to scan the samples. Cellular imaging with the TPM module (FV1200MPE-M, OLYMPUS, Japan) displayed the subcellular images and presented the glioma cells with the 20× objective. All of the TPM images were processed with *ZEN* software, which is one of the components of TPM. This TPM image showed the field-of-view of approximately 130×130×300 μm^3 *in vivo*. Due to the unlabeled normal cells, the TPM can only display the concentration degree of the tumor cells.

We used adult mice for the tumor cell inoculation. The procedure of the tumor cell inoculation included incision and dissection of the skin to open the skull, injecting the GBM cells into the orthotopic cerebral hemisphere and suturing the skin. Then, these mice were freely cultivated for weeks in the experimental environment.

In vivo GBM imaging with whole-body bioluminescence imaging for delineating and locating the GBMs

We tested the BLI image and provided the fluorescence intensity of the brain tumor at 1, 2, 5, and 10 s before BLI; these fluorescence intensities reached 3.05×10^5 p/sec/cm^2/sr, 1.73×10^6 p/sec/cm^2/sr, 5.26×10^6 p/sec/cm^2/sr, and 2.10×10^7 p/sec/cm^2/sr, respectively. The intensity was able to reach a maximum value. The duration was chosen as approximately 10 s to avoid photobleaching. We imaged the mice with orthotopic glioma using the whole-body BLI module and acquired the fluorescence intensity of the mouse model. We acquired the bioluminescence images of two mice during one-week, two-week and four-week timelines after the injection of GBM cells (**Figure 5A**). Furthermore, we used *LivingImaging* to delineate the GBM margin and automatically determine the fluorescence intensity. This delineation of GBMs was depicted using the area circled by the red line.

To evaluate tumor progression after the injection of human GBM cells, the BLI was performed, and the results showed that the size of the GBMs and the amount of tumor cells experienced a great change within approximately four weeks. At the one-, two- and four-week timepoints, the fluorescence intensities of mouse R1 were 6.69×10^7 p/sec/cm^2/sr, 1.04×10^8 p/sec/cm^2/sr, and 2.47×10^9 p/sec/cm^2/sr, respectively, and those of mouse R2 were 3.81×10^7 p/sec/cm^2/sr, 9.89×10^7 p/sec/cm^2/sr, and 8.36×10^9 p/sec/cm^2/sr. These results are shown in **Figure 5B**. The fluorescence intensity had a noticeable growth with changes in time. The results of BLI demonstrated that the progression of the GBMs significantly

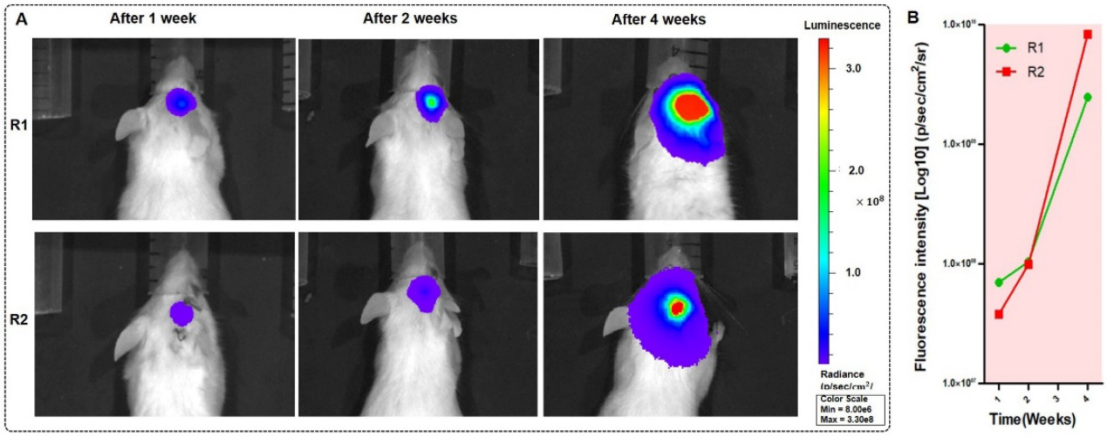

Figure 5. The BLI monitoring of the mice (R1 and R2) with GBMs a few weeks after tumor cell injection. (A-B) Two mice with *in vivo* BLI and the fluorescence intensity at 1 week, 2 weeks and 4 weeks after the orthotopic injection.

changed and that the size of the orthotopic tumors significantly increased (P=0.0027).

In vivo laser ablation evaluation experiments in a mouse model

The mouse model was prepared in the experimental environment. The evaluation experimental environment had two impact factors, the height H and the incidence angle θ. We set the height H as 0.0 mm, 0.5 mm, 1.0 mm, 1.5 mm and 2.0 mm and the incidence angle θ as 0°, 10°, 20°, and 30°.

The experimental environment is shown in **Figure 6A-B**. We set the initial radiation power and radiation duration to 5 W and 5 s, respectively. Then, the *in vivo* experimental implementation of laser ablation was conducted. The mice were in a state of anesthesia. After an evaluation experiment of the laser ablation with the optical theranostics platform, the mice were immediately sacrificed. The specimens (**Figure 6A-B**) were then immediately sent for histopathologic analysis. In this experiment, the labels 1, 2, 3, 4, and 5 in the height of the experimental environment (**Figure 6A**) correspond to H = 0.0 mm, 0.5 mm, 1.0 mm, 1.5 mm and 2.0 mm, respectively; the labels 1, 2, 3, and 4 in the incidence angle of the experimental environment (**Figure 6B**) correspond to θ = 0°, 10°, 20°, and 30°, respectively. The histopathological sections of the specimens are shown in **Figure 6C-D**, which correspond to the height and incidence angle of the evaluation experiment, respectively.

In the *in vivo* laser ablation of orthotopic GBMs, the laser-tissue parameters were conducted and measured in two groups of experiments. The height and the horizontal and longitudinal parameters are listed in **Table 1**. Similarly, in the evaluation experiment, the incidence angle and horizontal and longitudinal parameters are listed in **Table 2**. These parameters changed within the 0.1-1.0 mm range. The results demonstrate that the laser ablation accuracy reached a submicrometer level. In addition, the laser ablation accuracy met the needs of the tumor treatment within a certain margin of error, which is less than approximately 0.5 mm.

In vivo laser ablation with coupled ablated path planning under the guidance of BLI

In the treatment of orthotopic GBMs in living mice, we implemented laser ablation for brain orthotopic tumors with the guidance of BLI. Before laser ablation, we initialized the laser parameters, which were the initialized radiation power of 1 W and

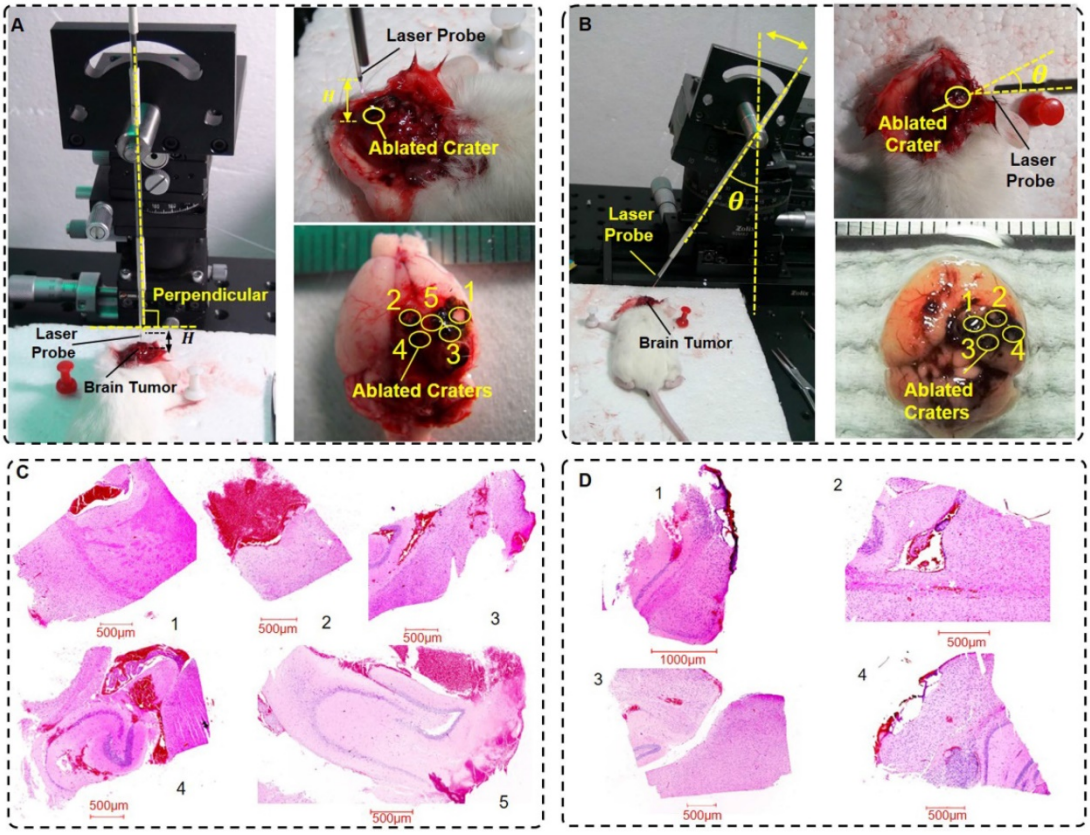

Figure 6. The experimental situation with different heights and angles of the fiber probe. (A-B) The experimental settings for the height and incidence angle of the fiber probe, respectively. **(C-D)** The histopathological sections in the evaluation situations of the different heights and incidence angles of the fiber probe, respectively (scale bar: 500 μm).

a radiation duration of 1 s. Furthermore, we chose the appropriate height and incidence angle of the laser-fiber probe in the laser ablation procedure.

Table 1. The height between the fiber probe and tissue interface evaluation experiment in the *in vivo* mouse GBMs

Label	1	2	3	4	5
Height (*H*, mm)	0	0.5	1.0	1.5	2.0
a (mm)	1.5	1.3	1.1	0.9	0.6
c (mm)	0.9	0.6	0.4	0.2	0.1

Table 2. The experimental evaluation of the incidence angle of the probe in a mouse model.

Label	1	2	3	4
Angle (θ, °)	0	10	20	30
a (mm)	1.2	1.0	0.8	0.6
c (mm)	0.5	0.3	0.2	0.1

Coupled ablated path planning is required for full field-of-view treatment and *in vivo* brain orthotopic tumors. Before laser ablation, we used BLI to measure the fluorescence intensity of GBMs (**Figure 7A**). In this study, we ablated one mouse orthotopic GBM using coupled ablated path planning for the laser ablation, and this laser ablation procedure is shown in **Figure 7B**). The mapping relationship between the laser parameters and the tumor boundary with BLI is listed in **Table 3**. The mapping relationship is described in the previous section. Additionally, a specimen of the whole brain was acquired, and histopathological sections were evaluated.

We acquired *in vivo* whole-body BLI of two mice GBMs before laser ablation, and the intensities of the regions of interest were 2.47×10^9 p/sec/cm²/sr and 4.70×10^8 p/sec/cm²/sr. Similarly, we also acquired *in vivo* whole-body BLI of the GBM post laser ablation, and the intensities of the regions of interest were 3.95×10^6 p/sec/cm²/sr and 2.59×10^6 p/sec/cm²/sr (**Figure 7C**), and therefore, the resection ratio reached 99.85% and 99.94%. These results demonstrate that the orthotopic GBMs were resected as much as possible with the guidance of BLI and that the residual tumor was negligible based on the fluorescence intensity.

Table 3. The mapping relationship between the laser parameters and the tumor boundary through the coupled ablated path.

Coupled ablated path	Laser parameters			
	H (mm)	θ (°)	*P* (W)	*T* (s)
Outside path	2.0 or 1.5	0	1~2	1~2
Intermediate path 1	1.0 or 0.5	0, 10 or 20	3~4	1~4
Intermediate path 2	1.0 or 0.5	0, 10 or 20	3~4	1~5
…	…	…	…	…
Inside path	0.0	20 or 30	5	5

Comparison of the histopathological sections and the TMP images

For evaluating the differences in *in vivo* laser ablation, experimental validation was conducted. TPM imaging and histopathological analysis of the GBM before and after laser ablation were implemented. To quantitatively analyze the GBM, BLI was also conducted, and the fluorescence intensity of the mouse brain tumor was automatically computed.

Figure 8 shows the BLI, TPM imaging and histopathological sections before laser ablation with the optical theranostics platform. TPM images show that the concentration of GBM cells is very high in the tumor area *in vivo*. **Figure 9** shows the TPM and BLI results after laser ablation with the optical theranostics platform. Histopathological sections were obtained to evaluate laser ablation. The ablated mouse tissue was imaged with the TPM and BLI module. From the TPM images, the concentration and

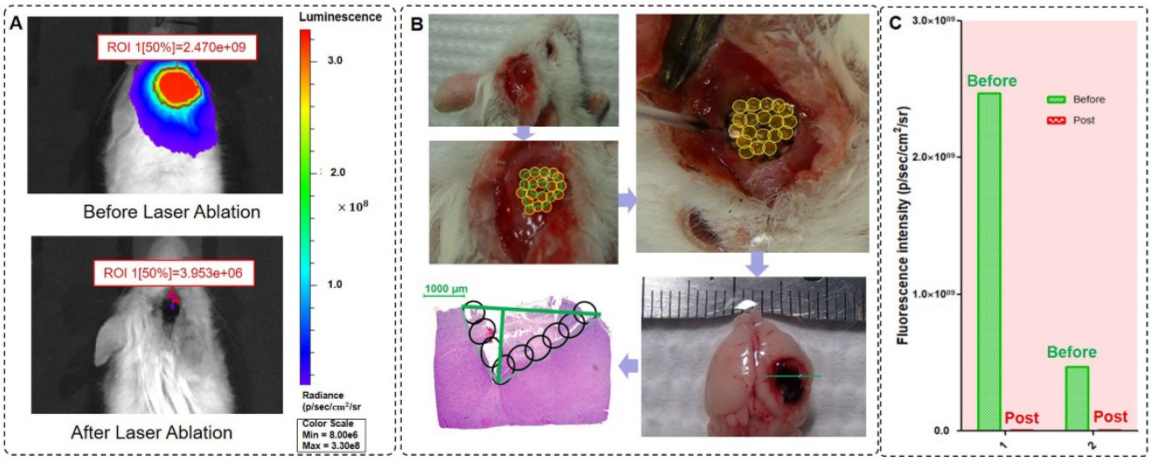

Figure 7. Laser ablation under the guidance of BLI and histopathological sections of the GBM after laser ablation. (A) The BLI before and after laser ablation with the optical theranostics platform. **(B)** The procedure of *in vivo* laser ablation and histopathological sections corresponding to the green line in the *ex vivo* specimens of brain tissues. **(C)** The fluorescence intensity of two mice before and after laser ablation with the optical theranostics platform.

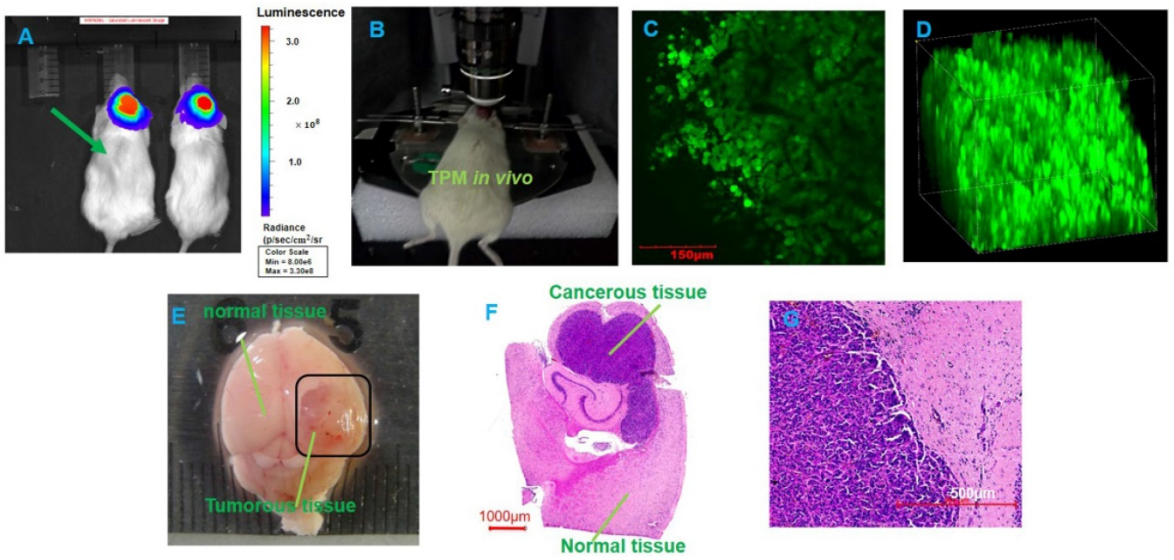

Figure 8. The two-photon microscopic imaging before the laser ablation of GBMs. (A) The BLI before laser ablation. **(B)** *In vivo* TPM imaging of a mouse tumor. **(C-D)** Two-dimensional and three-dimensional TMP images, respectively (scale bar: 150 μm). **(E)** The whole brain specimens from GBMs (scale bar: 1 mm). **(F-G)** The histopathological sections (scale bars: 1000 μm and 500 μm, respectively).

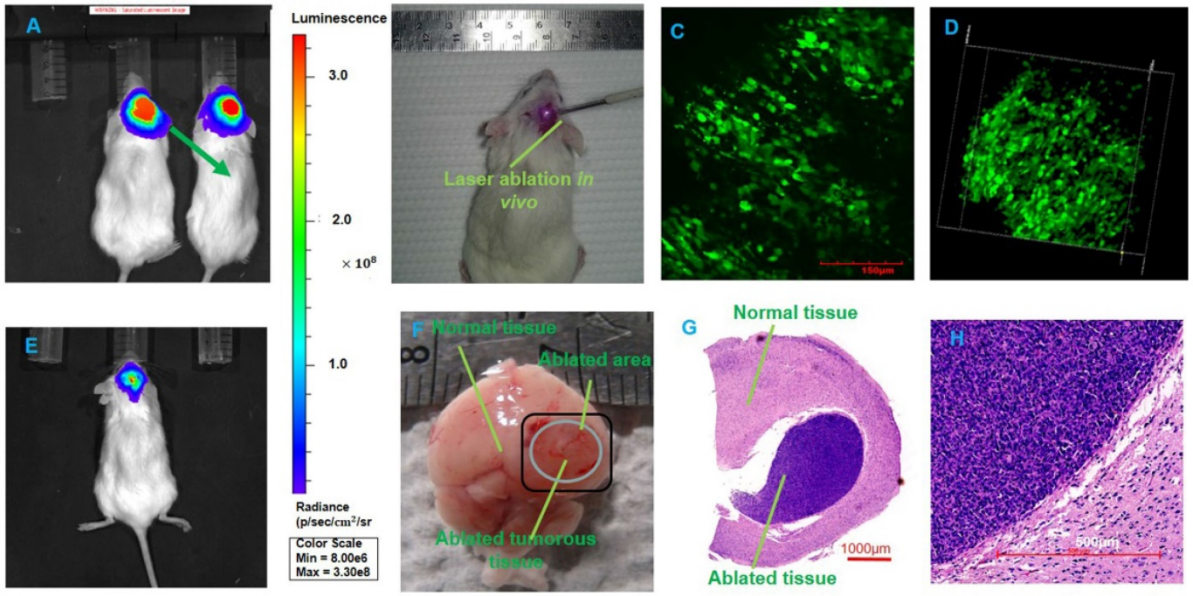

Figure 9. The TPM imaging after laser ablation. (A, E) The BLI before and post laser ablation *in vivo*, respectively. **(B)** *In vivo* laser ablation. **(C-D)** *In vivo* TPM imaging at the location of the tumor boundary with three-dimensional TPM images (scale bar: 150 μm). **(F)** The whole brain specimens *ex vivo* (scale bar: 1 mm). **(G-H)** The histopathological sections of ablated brain specimens (scale bars: 1000 μm and 500 μm, respectively).

cell numbers demonstrate that a significant difference existed before and after laser ablation. From the pathological section, the cellular structure of healthy and tumorous tissue is also significantly different.

Preventing local recurrence with the optical theranostics platform

In the validation experiment, the first cohort of mice were neoplastic and treated (tumor+/ablation+), the second cohort of mice were neoplastic and nontreated (tumor+/ablation-), and the third cohort of mice were healthy (tumor-/ablation-), corresponding to 6, 18, and 6 mice, respectively (**Figure 10A**). Four mice died in the early postoperative period. The wound was closed, and all of the mice were followed for local recurrence for approximately 60 days until all of the neoplastic mice died. The weights of all of the mice were measured. The weights of three cohorts are shown in **Figure 10B-D**. **Figure 10B** demonstrates that the weight loss of the first cohort was slower than that of the second cohort (**Figure 10C**) (P=0.0494). The weight of healthy mice was increased continuously (**Figure 10D**). The local recurrence is shown in **Figure 10E**. The third cohort was still alive. The mortality rate of the second cohort was significantly higher than that of

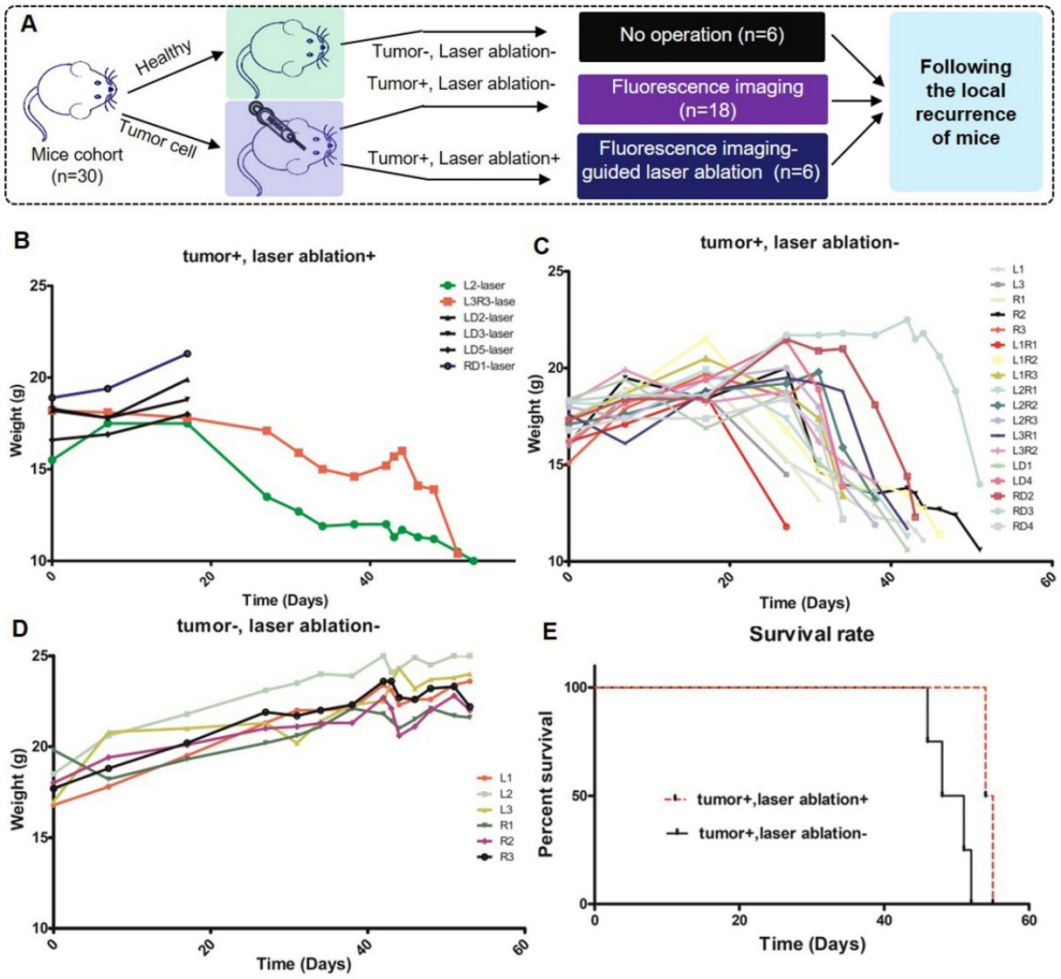

Figure 10. Physiological index of mice with the treatment of the optical theranostics platform in a local recurrence experiment. (A) The mice are divided into three cohorts, which include the healthy mouse cohort, the neoplastic and non-treated mouse cohort, and the neoplastic and treated mouse cohort. **(B-D)** The weights of the three cohorts corresponding to healthy, non-treated and treated cohorts.The labels distinguish different mice. **(E)** The survival rate of different cohorts.

the first cohort. These results demonstrate that the therapeutic effect of the optical theranostics platform is significant for the treatment of mouse brain tumors.

Discussion

In this study, the optical theranostics platform provided precise treatment for GBMs in a mouse model. The BLI provided delineation of the GBM margins and the fluorescence intensities of the *in vivo* mouse GBMs. This BLI information guided laser ablation for the treatment of GBMs using the coupled ablated path planning method. *In vivo* TPM imaging was conducted for orthotopic GBMs before and after laser ablation. The histopathological sections were also analyzed to evaluate the structure of the brain specimens.

Whole-body BLI monitors the progression of the brain intravital orthotopic glioma and provides a quantitative analysis. The BLI automatically delineates the tumor, and the fluorescence intensity displays the cell sizes and numbers. This quantitative analysis was conducted during the progression of intravital GBMs before and after laser ablation. Furthermore, BLI provides fluorescence intensity of the residual cancerous tissue and evaluates the ablated results of the GBMs treatment regarding a quantitative analysis. This BLI, which is used as a non-invasive monitoring tool for the quantitative evaluation of the progression and treatment of laser ablation, detected the GBMs with precise diagnosis and analysis. This method is limited to preclinical research. In the future, we will replace BLI with indocyanine green (ICG) [39], LUM015 [40], and intraoperative fluorescein [41] for intraoperative detection and analysis in clinical research and applications. Since tumors always have a three-dimensional (3D) structure, combination of fluorescence molecular tomography (FMT) and micro-computed tomography (μCT) will provides the 3D or whole-body model of tumor [42], future research will focus on the analysis of the 3D structure with optical coherence tomography [25] for real-time imaging and diagnosis.

In laser ablation, the height between the fiber

probe and the tissue surface significantly impacted the laser-tissue parameters. We conducted the experiment with height adjustment using five heights to evaluate the ablation and obtain the laser-tissue parameters. Similarly, the incidence angle of the fiber probe has important influence on the accuracy of laser ablation. We conducted the experiment of the incidence angle adjustment at four angles and acquired the laser-tissue parameters. Regarding the laser parameters, we controlled the radiation power and radiation duration for the laser ablation of *ex vivo* biological tissue in our previous studies [25, 43]. In this study, we proposed that the two factors also had some influence on laser ablation for *in vivo* GBMs. This design will improve the practicality and increase the feasibility of the laser treatment of *in vivo* brain orthotopic tumors. Laser ablation with the appropriate parameters will provide a precise treatment. Furthermore, in future research, a finer height and incidence angle will be determined and more data will be acquired to provide detailed data and guide laser ablation.

TPM provides microscopic imaging analysis and allows sub-cellular imaging of the tumor cells. Within a certain field-of-view, the TPM images provide the concentration and cell numbers of GBMs. We conducted the experiment with TPM imaging and histological analysis for the treatment evaluation of *in vivo* GBMs. The field-of-view of TPM imaging is limited within hundreds of microns, and this view provides some local glioma cell numbers and the concentration degree of glioma cells.

From the clinical application point of view, magnetic resonance imaging (MRI) and computer tomography (CT) cannot currently achieve real-time imaging and diagnosis of diseased tissue. MRI and CT are usually used as the preoperative imaging modalities to assist neurosurgery. Fluorescence imaging can provide intraoperative diagnosis and guidance for integration into the theranostics system. Similarly, bioluminescence imaging has the feature of being useful for intraoperative imaging and diagnosis. This imaging is only in the early stage of a feasibility study with preclinical research. In a future clinical application, the same solution could be used in translational medicine.

A fluorescence-guided laser-ablation system was proposed by Liao *et al*., and this system has a clear purpose, i.e., for treatment of GBMs. We also developed the integration of optical-coherence tomography and a laser-ablation system for surgical treatment, and this system has the potential for use in neurosurgical treatment. Intelligent neurosurgical devices [44, 45] will partially take the place of surgical resections and solve the brain deep-tumor treatment problem. Furthermore, the integration of multimodality imaging and laser ablation will improve the efficiency of laser ablation. The optical theranostics platform, including BLI, intraoperative imaging and diagnosis, electrophysiological monitoring [46] and laser ablation, will be integrated into a system that can provide precise diagnosis and therapeutics for brain orthotopic GBMs and diffuse intrinsic pontine glioma (DIPG). Fluorescence imaging for real-time delineation of the tumor boundary to determine laser ablation parameters should be integrated into the system. A robotic arm-assisted fiber probe for the laser, which treats tumorous tissues with the guidance of BLI and TPM, should be designed and programmatically controlled. Machine vision should be developed as a tool for real-time visualization of the tumor tissue.

Conclusion

We developed an optical theranostics platform with BLI- and TPM-guided laser ablation and coupled ablated path planning for the *in vivo* treatment of mouse brain orthotopic tumors. This method provides an approach for GBM treatment in a mouse model. The multimodality imaging-guided laser ablation has great potential for clinical application and for minimally invasive theranostics [44] of brain orthotopic tumors such as the treatment of GBMs.

This study provides a possibility for bridging the gap of fundamental research and clinical applications regarding neurosurgical guidance with BLI and TPM imaging. In the future, intraoperative multimodalities for identification and analysis will be integrated into this optical theranostics platform. This integration can provide more information for the diagnosis and delineation of glioma margins and intraoperative identification.

Abbreviations

GBMs: glioblastoma multiforms; BLI: bioluminescence imaging; TPM: two-photon microscopy; MRI: magnetic resonance imaging; CT: computer tomography; OCT: optical coherence tomography; 5-ALA: 5-aminolevulinic acid; CARS: coherence anti-Stokes Raman scattering; GFP: green fluorescence protein; H&E: hematoxylin and eosin; PAI: photoacoustic imaging; ICG: indocyanine green; FMT: fluorescence molecular tomography; μCT: micro-computed tomography; DIPG: diffuse intrinsic pontine glioma.

Acknowledgements

This work was partially funded by Beijing Municipal Science & Technology Commission (Z151100003915079), Beijing Municipal Natural

Science Foundation (7172122, L172003), National Key Research and Development Program of China (2017YFC0108000), National Natural Science Foundation of China (81427803, 81771940), and Beijing municipal administration of Hospitals Clinical Medicine Development of Special Funding Support (ZYLX201608). Authors thank Laboratory Animal Research Center in Tsinghua University for technical support to histopathological section. Authors thank Center of Biomedical Analysis in Tsinghua University for technical support to digital pathological scanning and TPM imaging.

Competing Interests

The authors have declared that no competing interest exists.

References

1. Wirth D, Kolste K, Kanick S, Roberts DW, Leblond F, and Paulsen KD. Fluorescence depth estimation from wide-field optical imaging data for guiding brain tumor resection: a multi-inclusion phantom study. Biomed. Opt. Express. 2017; 8: 3656-3670.
2. Azagury DE, Dua MM, Barrese JC, Henderson JM, Buchs NC, Ris F, et al. Image-guided surgery. Current Problems in Surgery. 2015; 52(12): 476-520.
3. Ji M, Orringer DA, Freudiger CW, Ramkissoon S, Liu X, Lau D, et al. Rapid, label-free detection of brain tumors with stimulated Raman scattering microscopy. Science Translational Medicine. 2013; 5.201:921-925.
4. Silva D, Sharma M, Barnett GH. Laser ablation vs open resection for deep-seated tumors: evidence for laser ablation. Neurosurgery. 2016; 63 (CN_suppl_1): 15-26.
5. Fan Y, Xia Y, Zhang X, Sun Y, Tang J, Zhang L, et al. Optical coherence tomography for precision brain imaging, neurosurgical guidance and minimally invasive theranostics. BioScience Trends. 2018; 12(1):12-23.
6. Rodriguez A, Tatter SB. Laser ablation of recurrent malignant gliomas: current status and future perspective. Neurosurgery. 2016; 79 (suppl_1): S35–S39.
7. Hawasli AH, Kim AH, Dunn GP, Tran DD, Leuthardt EC. Stereotactic laser ablation of high-grade gliomas. Neurosurg Focus. 2014; 37(6):E1.
8. Lee I, Kalkanis S, Hadjipanayis CG. Stereotactic laser interstitial thermal therapy for recurrent high-grade gliomas. Neurosurgery.2016; 79 (suppl_1): S24–S34.
9. Lagman C, Chung LK, Pelargos PE, Ung N, Bui TT, Lee SJ, et al. Laser neurosurgery: A systematic analysis of magnetic resonance-guided laser interstitial thermal therapies. Journal of Clinical Neuroscience. 2017; 36: 20-26.
10. Schwartz JA, Shetty AM, Price RE, Stafford RJ, Wang JC, Uthamanthil RK, et al. Feasibility study of particle-assisted laser ablation of brain tumors in orthotopic canine model. Cancer Research. 2009; 69(4): 1659.
11. Bisdas S, Roder C, Ernemann U, Tatagiba MS. Intraoperative MR Imaging in Neurosurgery. Clin Neuroradiol. 2015; 25: 237.
12. Zausinger S, Schichor C, Uhl E, Reiser MF, and Tonn JC. Intraoperative CT in Neurosurgery. Intraoperative Imaging and Image-Guided Therapy. 2014:529-536.
13. Pedro MT, Antoniadis G, Scheuerle A, Pham M, Wirtz CR, Koenig RW. Intraoperative high-resolution ultrasound and contrast-enhanced ultrasound of peripheral nerve tumors and tumorlike lesions. Neurosurgical Focus. 2015; 39.3.
14. Karabeber H, Huang R, Iacono P, Samii JM, Pitter K, Holland EC, et al. Guiding brain tumor resection using surface-enhanced Raman scattering nanoparticles and a hand-held Raman scanner. ACS Nano. 2014; 8(10): 9755–9766.
15. Viet-Hoan Le, Yoo SW, Yoon Y, Wang T, Kim B, Lee S, et al. Brain tumor delineation enhanced by moxifloxacin-based two-photon/CARS combined microscopy. Biomed. Opt. Express. 2017; 8: 2148-2161.
16. Ji M, Lewis S, Camelo-Piragua S, Ramkissoon SH, Snuderl M, Venneti S, et al. Detection of human brain tumor infiltration with quantitative stimulated Raman scattering microscopy. Science Translational Medicine. 2016; 78.309:829-831.
17. Kut C, Chaichana KL, Xi J, Raza SM, Ye X, McVeigh ER, et al. Detection of human brain cancer infiltration ex vivo and in vivo using quantitative optical coherence tomography. Science Translational Medicine. 2015; 7(292):292ra100.
18. Kairdolf BA, Bouras A, Kaluzova M, Sharma AK, Wang MD, Hadjipanayis CG, et al. Intraoperative spectroscopy with ultrahigh sensitivity for image-guided surgery of malignant brain tumors. Analytical Chemistry. 2016; 88(1): 858.
19. Ravì D, Fabelo H, Callic GM and Yang GZ. Manifold embedding and semantic segmentation for intraoperative guidance with hyperspectral brain imaging. IEEE Transactions on Medical Imaging. 2017; 36(9): 1845-1857.
20. Chi C, Du Y, Ye J, Kou D, Qiu J, Wang J, et al. Intraoperative imaging-guided cancer surgery: from current fluorescence molecular imaging methods to future multi-modality imaging technology. Theranostics. 2014; 4(11):1072-1084.
21. Balog J, Sasi-Szabó L, Kinross J, Lewis MR, Muirhead LJ, Veselkov K, et al. Intraoperative tissue identification using rapid evaporative ionization mass spectrometry. Science Translational Medicine. 2013; 5.194:153-154.
22. Liao H, Shimaya K, Wang K, Maruyama T, Noguchi M, Muragaki Y, et al. Combination of intraoperative 5-aminolevulinic acid induced fluorescence and 3-D MR imaging for guidance of robotic laser ablation precision neurosurgery. 11th International Conference on Medical Image Computing and Computer-Assisted Intervention—MICCAI 2008. Lect Notes Comput Sci. 2008; 5242:373–380.
23. Liao H, Noguchi M, Maruyama T, Muragaki Y, Kobayashi E, Iseki H, et al. An integrated diagnosis and therapeutic system using intraoperative 5-Aminolevulinic-Acid-induced fluorescence guided robotic laser ablation for precision neurosurgery. Med Image Anal. 2012; 16(3): 754-766.
24. Lagman C, Chung LK, Pelargos PE, Ung N, Bui TT, Lee SJ, et al. Laser neurosurgery: A systematic analysis of magnetic resonance-guided laser interstitial thermal therapies. Journal of Clinical Neuroscience. 2017; 36: 20-26.
25. Fan Y, Zhang B, Chang W, Zhang X, Liao H. A novel integration of spectral-domain optical-coherence-tomography and laser-ablation system for precision treatment. International Journal of Computer Assisted Radiology and Surgery. 2017; 13(3):411-423.
26. Lazarides AL, Whitley MJ, Strasfeld DB, Cardona DM, Ferrer JM, Mueller JL, et al. A fluorescence-guided laser ablation system for removal of residual cancer in a mouse model of soft tissue sarcoma. Theranostics. 2016; 6(2):155-166.
27. Liu H, Xie Y, Zhang Y, Cai Y, Li B, Mao H, et al. Development of a hypoxia-triggered and hypoxic radiosensitized liposome as a doxorubicin carrier to promote synergetic chemo-/radio-therapy for glioma. Biomaterials. 2017; 121:130-143.
28. Hashizume R, Ozawa T, Dinca EB, Banerjee A, Prados MD, James CD, et al. A human brainstem glioma xenograft model enabled for bioluminescence imaging. Journal of Neuro-Oncology. 2010; 96(2): 151–159.
29. Mittra ES, Fan-Minogue H, Lin FI, Karamchandani J, Sriram V, Han M, et al. Preclinical efficacy of the anti-hepatocyte growth factor antibody Ficlatuzumab in a mouse brain orthotopic glioma model evaluated by bioluminescence, PET, and MRI. Clinical Cancer Research. 2013; 19(20): 5711–5721.
30. Xi L, Zhou G, Gao N, Yang L, Gonzalo DA, Hughes SJ, et al. Photoacoustic and fluorescence image-guided surgery using a multifunctional targeted nanoprobe. Annals of Surgical Oncology. 2014; 21(5), 1602–1609.
31. Rodney B. Luwor, Stanley S. Stylli, Andrew H. Kaye. Using bioluminescence imaging in glioma research. Journal of Clinical Neuroscience. 2015; 22(5): 779-784.
32. Li X, Schumann C, Albarqi HA, Lee CJ, Alani AWG, Bracha S, et al. A tumor-activatable theranostic nanomedicine platform for NIR fluorescence-guided surgery and combinatorial phototherapy. Theranostics. 2018; 8(3): 767-784.
33. Zong W, Wu R, Li M, Hu Y, Li Y, Li J, et al. Fast high-resolution miniature two-photon microscopy for brain imaging in freely behaving mice. Nature Methods. 2017; 14(7): 713-719.
34. Sun H, Kurtz RM, Juhasz T. Evaluation of human sclera after femtosecond laser ablation using two photon and confocal microscopy. Journal of Biomedical Optics. 2012; 17(8): 081411.
35. Yang Z, Xie W, Ju F, Khan A, Zhang S. Two-photon imaging reveals a role of progesterone in reducing axonal dieback after spinal cord injury in mice. Neuropharmacology. 2017; 116:30-37.
36. Madden KS, Zettel ML, Majewska AK, Brown EB. Brain tumor imaging: live imaging of glioma by two-photon microscopy. Cold Spring Harb Protoc; 2013. (doi:10.1101 /pdb.prot073668).
37. Ricard C, Stanchi F, Rougon G, and Debarbieux F. An orthotopic glioblastoma mouse model maintaining brain parenchymal physical constraints and suitable for intravital two-photon microscopy. Journal of Visualized Experiments : JoVE. 2014; 86: 51108.
38. Sarkaria JN, Yang L, Grogan PT, Kitange GJ, Carlson BL, Schroeder MA, et al. Identification of molecular characteristics correlated with glioblastoma sensitivity to EGFR kinase inhibition through use of an intracranial xenograft test panel. Molecular cancer therapeutics. 2007; 6(3):1167-74.
39. Suganami A, Iwadate Y, Shibata S, Yamashita M, Tanaka T, Shinozaki N, et al. Liposomally formulated phospholipid-conjugated indocyanine green for intra-operative brain tumor detection and resection. International Journal of Pharmaceutics. 2015; 496(2): 401-406.
40. Whitley MJ, Cardona DM, Lazarides AL, Spasojevic I, Ferrer JM, Cahill J, et al. A Mouse-human Phase I co-clinical trial of a protease-activated fluorescent probe for imaging cancer. Science Translational Medicine. 2016; 8(320):320ra4.
41. Catapano G, Sgulò FG, Seneca V, Lepore G, Columbano L, di Nuzzo G. Fluorescein-guided surgery for high-grade glioma resection: an intraoperative "contrast-enhancer". World Neurosurgery. 2017; 104: 239-247.

42. Al Rawashdeh W, Zuo S, Melle A, Appold L, Koletnik S, Tsvetkova Y, et al. Noninvasive Assessment of Elimination and Retention using CT-FMT and Kinetic Whole-body Modeling. Theranostics; 2017; 7(6):1499-1510.
43. Su B, Tang J, Liao H. Automatic laser ablation control algorithm for an novel endoscopic laser ablation end effector for precision neurosurgery. Intelligent Robots and Systems (IROS), IEEE/RSJ International Conference on, Hamburg. pp. 4362-4367. (2015).
44. Liao H, Fujiwara K, Ando T, Maruyama T, Kobayashi E, Muragaki Y, et al. Automatic laser scanning ablation system for high-precision treatment of brain tumors. Laser in Medical Science. 2013; 28: 891-900.
45. Liao H. Integrated diagnostic and therapeutic techniques: Toward an intelligent medical system. Computerized Medical Imaging and Graphics. 2014; 38(5):421-422.
46. Acioly MA, Liebsch M, de Aguiar PH, Tatagiba M. Facial nerve monitoring during cerebellopontine angle and skull base tumor surgery: a systematic review from description to current success on function prediction. World Neurosurgery. 2013; 80(6): e271-e300.